Published in final edited form as:
Stem Cells. 2011 February ; 29(2): 286–296. doi:10.1002/stem.581.

Locally applied VEGFA increases the osteogenic healing capacity of human adipose derived stem cells by promoting osteogenic and endothelial differentiation

Björn Behr[a,b], **Chad Tang**[c], **Günter Germann**[b], **Michael T. Longaker**[a,*], and **Natalina Quarto**[a,d,*]

[a] Children's Surgical Research Program, Department of Surgery, Division of Plastic and Reconstructive Surgery, Stanford University School of Medicine, Stanford, CA, USA

[b] BG-Unfallklinik Ludwigshafen, Department of Plastic- and Handsurgery, University of Heidelberg, Germany

[c] Department of Pathology, Developmental Biology and Institute for Stem Cell Biology and Regenerative Medicine, Stanford University, Stanford, CA, USA

[d] Department of Structural and Functional Biology, University of Naples Federico II, Complesso M. S. Angelo, Napoli, Italy

Abstract

Human adipose derived stem cells (hASCs) are known for their capability to promote bone healing when applied to bone defects. For bone tissue regeneration, both sufficient angiogenesis and osteogenesis is desirable. Vascular endothelial growth factor A (VEGFA) has the potential to promote differentiation of common progenitor cells to both lineages. To test this hypothesis, the effects of VEGFA on hASCs during osteogenic differentiation were tested *in vitro*. In addition, hASCs were seeded in murine critical-sized calvarial defects locally treated with VEGFA. Our results suggest that VEGFA improves osteogenic differentiation *in vitro* as indicated by alkaline phosphatase activity, alizarin red staining, and QRT-PCR analysis. Moreover, local application of VEGFA to hASCs significantly improved healing of critical sized calvarial defects *in vivo*. This repair was accompanied by a striking enhancement of angiogenesis. Both paracrine and, to a lesser degree, cell-autonomous effects of VEGFA treated hASCs were accountable for angiogenesis. These data were confirmed by utilization of $CD31^-/CD45^-$ mouse $ASCs^{GFP+}$ cells. In summary, we demonstrated that VEGFA increased osteogenic differentiation of hASCS *in vitro* and *in vivo*, which was accompanied by an enhancement of angiogenesis. Additionally, we showed that during bone regeneration, the increase in angiogenesis of hASCs upon treatment with VEGFA was attributable to both paracrine and cell-autonomous effects. Thus, locally applied VEGFA might

*Correspondence Natalina Quarto : quarto@unina.it Michael T Longaker: longaker@stanford.edu 257 Campus Drive, Stanford, CA 94305-5148 USA phone: (650) 736-1704 fax: (650) 736-1705.

Author contributions:
Björn Behr: Conception and design, Collection of data, Data analysis and interpretation, manuscript writing, Final approval of manuscript
Chad Tang: Collection of data, Data analysis and interpretation, Final approval of manuscript
Günter Germann: Data analysis and interpretation, Final approval of manuscript
Michael T. Longaker: Conception and design, Financial support, Administrative support, Data analysis and interpretation, Final approval of manuscript
Natalina Quarto: Conception and design, Collection of data, Data analysis and interpretation, Final approval of manuscript

DISCLOSURE OF POTENTIAL CONFLICTS OF INTEREST
The authors indicate no potential conflicts of interest.

prove to be a valuable growth factor that can mediate both osteogenesis and angiogenesis of multipotent hASCs in the context of bone regeneration.

Keywords

VEGFA; Bone Regeneration; Angiogenesis; Endothel; Calvaria

INTRODUCTION

Human adipose derived stem cells (hASCs) are an attractive cell source for tissue engineering. They are easy to harvest by liposuction and available in great abundance, which potentially renders a period of *in-vitro* expansion unnecessary. Among various lineages, ASCs can also differentiate into the osteoblast lineage [1-8]. A fundamental step in bone tissue regeneration is a sufficient vascular supply since implantation of large bone grafts without adequate vascularity results in apoptosis and cartilage formation [9]. Accordingly, bone repair has been shown to benefit from increased angiogenesis [10]. In addition to their capability to differentiate to osteoblasts, hASCs are thought to have the capacity to differentiate to endothelial cells [11-13].

In a previous study, we have successfully increased bone healing in murine critical sized calvarial defects with non-differentiated mouse ASCs [5]. We sought to advance this concept and intended to promote both angiogenesis and osteogenic differentiation to facilitate bone healing. A factor that can potentially fulfill both requirements is vascular endothelial growth factor A (VEGFA). VEGFA is mainly known to induce angiogenesis [14], but can also promote osteogenesis [15, 16]. In development, VEGFA has been considered of great importance for the vascularization and patterning of the bone growth plate [17] and has also been shown as an integral part of a crosstalk between osteoblasts and endothelial cells [18]. VEGFA has been shown to increase bone formation in long bone defect models [15, 16], promote osteoblast differentiation in an autocrine fashion [15], inhibit osteoblast apoptosis [19], and induce endothelial cells from human embryonic stem cells [20, 21].

In the current study, we investigated the effects of VEGFA on multipotent hASCs during osteogenic differentiation *in vitro* and *in vivo*. Collectively, our data indicate that treatment of hASCs with VEGFA promotes osteogenesis and angiogenesis during calvarial healing.

MATERIALS & METHODS

Cell harvest and cell culture

Human ASCs were obtained from lipoaspirates of patients after informed consent, following approved guidelines by the Stanford University's Institutional Review Board. Primary cell culture of hASCs was performed as previously described [3, 8]. Briefly, lipoaspirates were washed with sterile PBS and digested with 0.075% Collagenase I (Sigma-Aldrich, St. Louis, MO) for 60 min in a shaking water bath at 37°C. Collagenase was inactivated with DMEM-GlutaMAX (GIBCO®, Invitrogen, Carlsbad, CA) medium containing 10% fetal bovine serum (FBS) (Invitrogen) and subsequently centrifuged at low speed. The pellet was resuspended in DMEM-GlutaMAX medium and filtered through a 100 μm nylon mesh to remove debris. The filtrate was re-centrifuged, cells were plated on regular tissue culture plates and cultured in DMEM-GlutaMAX medium containing 10%FBS and 100 IU/ml Penicillin/Streptomycin (Invitrogen) in incubators at 37°C and 5% atmospheric CO_2. Cells were passaged upon reaching subconfluence via a 5 min 37°C incubation in 0.25% trypsin (Invitrogen). $mASCs^{GFP+}$ were harvested from inguinal fat pads of in-house bred mice as

previously described, [5]. In these mice, enhanced GFP (EGFP) cDNA is under the control of a constitutively active chicken beta-actin promoter and cytomegalovirus enhancer [22]. For all experiments passage p0 and p1 cells were used.

Osteogenic differentiation of hASCs was induced by culturing hASCs with DMEM-GlutaMAX medium containing 10%FBS, 100 IU/ml Penicillin/Streptomycin, 10 mM β-glycerophosphatase and 100 μg/ml ascorbic acid (Sigma Aldrich). Moreover, when indicated, recombinant human VEGFA 165 (R&D Systems, Minneapolis, MN) was added to the osteogenic differentiation medium. During osteogenic differentiation, medium was changed every third day. Cells were seeded in triplicates for each experiment.

Alkaline phosphatase activity and mineralization assay

Alkaline phosphatase activity and Alizarin red mineralization staining were performed as previously described [23, 24]. Briefly, alkaline phosphatase activity was determined by biochemical colorimetric assay using Alkaline Phosphatase kit (#104-LS, Sigma-Aldrich) according to the manufacturer's instructions. After seeding cells in equal quantity (80,000 per well in a 6-well plate) and growing them to confluence, osteogenic differentiation was initiated. After 7 days of osteogenic differentiation, alkaline phosphatase activity was determined in cell lysates by measuring levels of *p*-nitrophenol, a metabolite formed during hydrolysis, via optical density measurements read at 420 nm. Values were normalized against protein concentration using a BCA protein assay kit (Pierce Biotechnology, Rockford, IL). Samples were run in triplicate. For Alizarin red staining, cells were fixed in neutral buffered formalin for 30 min, washed and stained with 0.2% Alizarin red for 30 min. Cells were then air-dried and evaluated by light microscopy. Quantification was performed with a colorimetric assays by incubating cells with 20% Methanol / 10% acetic acid solution for 15 min to elute calcium. Optical density was determined at 450 nm. Values were normalized against protein concentrations obtained from triplicate wells.

RNA isolation and quantitative Real-Time PCR

RNA was harvested with TRIzol (Invitrogen) according to the manufacturer's protocol. Purified RNA was then treated with DNAseI (Ambion, Austin, TX) and reversed transcribed to cDNA using random hexamers and SuperScript III reverse transcriptase according to the manufacturer's protocol (both Invitrogen). Quantitative real time PCR (qRT-PCR) was performed using the Applied Biosystems Prism 7900 HT sequence detection system and SYBR Green master mix. Primers were designed with the assistance of PrimerBank and are listed in **Table 1**. All PCR products were run on a 2% Agarose gel to determine appropriate size and specificity. Expression levels were normalized to *GAPDH* and reactions were performed in triplicates.

Flow cytometry

In order to separate GFP^+ mouse ASCs from contaminating CD31/CD45 cells during the cell harvest procedure, flow cytometry was inserted as an additional step. Instead of plating the cell pellet after the standard mASC harvesting procedure [5], cells were resuspended in FACS Buffer (5% FBS in PBS), incubated with APC anti-mouse CD45 (#559864) and APC anti-mouse CD31 (#551262) (dilution 1:200, BD Pharmingen, San Jose, CA, and resuspended in DAPI to exclude dead cells. To estimate non-specific binding, rat APC IgG2a and APC IgG2b (#400511/ #400611, dilution 1:200, BioLegend, San Diego, USA) were used as isotype controls.

First passage human cells were lifted in 0.25% trypsin for 5 min at 37°C and suspended in PBS with 2% FBS. Cells were incubated with Pacific Blue anti-human CD45 (#304029) and Pacific Blue anti-human CD31 (#303114) (both 1:200 and from BioLegend, San Diego, CA)

and resuspended in propidium iodide (PI) to exclude dead cells. To estimate non-specific binding, mouse Pacific Blue IgG1 (#400151, 1:200, BioLegend) was used as an isotype control. Cells were passed through a 40 μm strainer and sorted on a FACS Aria II (BD) using a 100 μm nozzle. Forward scatter area/width and side scatter area was used to exclude debris and doublets and PI or DAPI were used to exclude dead cells.

Cell seeding on scaffolds

hASCs were trypsinized, washed with FBS and counted. 1.5×10^6 hASCs or CD31$^-$/CD45$^-$ mASCs^{GFP+} were treated with 2μg recombinant human VEGFA 165 (R&D Systems) or left untreated and seeded on 6 mg of Pro Osteon 200R coral scaffolds (Interpore, Irvine, CA), which were previously described for their use in osteogenic differentiation of human mesenchymal cells [25]. In order to best mimic potential clinical translational scenarios, scaffolds were implanted in calvarial defects 20 min after *in vitro* seeding. The same procedure was utilized to seed CD31$^-$/CD45$^-$ mASCs^{GFP+} cells.

Animal Surgery

All animal experiments were performed in accordance with Stanford University Animal Care and Use Committee guidelines. For evaluating the *in vivo* healing capacity of VEGFA treated hASCs and angiogenesis of CD31$^-$/CD45$^-$ mASCs^{GFP+} cells, 50 day-old male nude CD1-mice (Charles River Laboratories, Wilmington, MA) underwent calvarial defect procedures. After anesthesia with an intraperitoneal injection of ketamine 100 mg/kg + xylazine 20 mg/kg + acepromazine 3 mg/kg and disinfection of the surgical site of the mice, 4-millimeter defects were created with a trephine drill bit in left parietal bones as previously described [26]. Meticulous care was taken in order to protect the underlying dura mater or neighboring cranial sutures. Treatment groups included no treatment (empty), scaffold with serum, scaffold with 2μg hVEGFA 165 + serum, scaffold seeded with hASCs and scaffold seeded with 2μg of hVEGFA 165 treated hASCs. The scaffolds were placed in the defects, the wound was closed, and the animals were allowed to recover.

μCT-scanning

μCT-scanning was performed as previously described [26]. Briefly, CD1 nude mice were scanned with a high-resolution MicroCAT II™ scanner (ImTek Inc., Knoxville, TN) with an X-ray voltage of 80 kVP and an anode current of 450 μA. A resolution of 80 μm was obtained with 144 steps over 360° rotation. X-ray data reconstruction was performed with Cobra EXXIM, (EXXIM Computing Corp., Livermore, CA) and Micro View Software (GE Healthcare, London, Canada). Each mouse was scanned with a CT-phantom, which was used to calibrate each scan. The precise threshold for regenerating calvarial bone was previously determined equivalent to 510 Houndsfield Units. The rest-defect area was then determined with the Magic Wand Tool in Photoshop (Adobe). Percentage healing was determined by dividing the rest defect area by the mean of the defect size one day postoperatively. CD1 nude mice were scanned at week 1, 2, 4 and 8. For statistical analysis, the VEGFA treated hASCs group was compared with all other groups using the Mann-Whitney test. A p-value < 0.05 was considered statistically significant.

Histology, immunohistochemistry and immunofluorescence

Skulls were harvested under a stereomicroscope and fixed in 10% neutral buffered formalin overnight and decalcified in 19% EDTA. For immunofluorescence experiments, mice were intracardially perfused with 4% PFA, skulls were harvested, fixed in 4% PFA at 4°C overnight and decalcified. Samples were then dehydrated and paraffin embedded. Hematoxylin, Hematoxylin and Eosin (H&E), Aniline Blue and Pentachrome staining was performed according to standard procedures. Moreover, histomorphometric measurements

to quantify the regenerate bone were performed using Adobe Photoshop on every 6th Aniline Blue stained slide of the defect as previously described [27]. Staining for tartrate-resistant acid phosphatase (TRAP) was performed as previously described [27]. Immunohistochemistry for Runx2 (#SC-10758, Santa Cruz Biotechnologies, Santa Cruz, CA 1:50), platelet endothelial cell adhesion molecule (PECAM-1) against mouse (#553370, BD-Pharmingen, San Diego, CA 1:400) and proliferating cell nuclear antigen (PCNA) (#93-1143, Invitrogen) was performed as previously described [26]. Briefly, paraffin-embedded samples were cut in 8 μm sections, rehydrated, treated with Proteinase K for 10 min and incubated with the primary antibody at 4°C overnight. Subsequently, the respective secondary antibody was added and sections were developed with NovaRed (Vectorlabs, Burlingame, CA). As an exception, immunohistochemistry for human PECAM-1 staining (#IS610, Dako North America, ready to use) was performed with heat antigen retrieval in citrate buffer (pH 6.0). For PCNA staining, a kit was utilized. In order to detect transplanted mASCs^{GFP+} and co-localize with PECAM-1 staining, confocal microscopy was performed. Sections were incubated in mouse PECAM-1 primary antibody at 4°C overnight, followed by incubation with Alexa Fluor 594 goat anti-rat secondary antibody (Invitrogen, 1:400) for one hour. Coverslips were applied with Vectashield Mounting media (Vectorlabs) and analyzed either with a fluorescence (Axioplan, Zeiss) or confocal fluorescence microscope (Leica DM IRE2). Vessels were counted or quantified on at least 7 stained slides per defect by two blinded independent examiners at 5x magnification. Vessels were defined by their positive PECAM-1 stain and their typical round or oval structure containing a lumen. Vessel surface was histomorphometrically quantified. Pixel count was partially automated with the magic wand tool in Adobe Photoshop (settings: tolerance 60%; no-contiguous). This tolerance setting resulted in highlighted pixels that corresponded exactly to the PECAM-1 positive endothelial cells as defined by their round or oval structure containing a lumen. Highlighted areas that did not fulfill these vessel criteria were manually deselected. Means and standard deviations were calculated for each group and Mann-Whitney test was used for statistical analysis. Data represent the mean of three independent experiments. Moreover, in order to determine the proportion of GFP positive cells in relation to the entire cell population within a calvarial defect, at least 5 slides per defect cover slipped with Vectashield Mounting media (Vectorlabs) were photographed at 20x with a fluorescence microscope (Axioplan, Zeiss). GFP-positive and DAPI positive cells were counted within the entire defect (between the bony edges) by two blinded independent examiners. A proportion was calculated by dividing GFP-positive cells by DAPI cells. The result is presented as mean ± standard deviation.

RESULTS

In vitro analysis of osteogenic differentiation

As a first step, we analyzed the effects of VEGFA during osteogenic differentiation. Enzymatic alkaline phosphatase assay revealed that activity in hASCs undergoing osteogenic differentiation in the presence of VEGFA was 123% higher for 20 ng/ml VEGFA and 139% higher for 200 ng/ml VEGFA at day 7 (**Figure 1A)**. Alizarin red staining, which detects mineralization of extracellular matrix at later time points, paralleled these findings at day 14 (**Figure 1B)**. After spectromorphometric quantification and protein normalization, hASCs undergoing osteogenic differentiation in the presence of 20 ng VEGFA showed an increase in extracellular matrix mineralization of 129%, 200 ng VEGFA led to an increase of 135% as compared to no addition of VEGFA.

In order to verify whether the *in vitro* effects of VEGFA would be mirrored by gene expression of osteogenic markers, we performed qRT-PCR analysis at day 0, 3, 7 and 14 (**Figure 1C)**. Expression of *RUNX-2*, an early osteogenic marker, doubled in VEGFA

treated hASCs at day 3 and 7 as compared to untreated hASCs undergoing osteogenic differentiation. Analysis for *OSTEOCALCIN*, a late osteogenic marker, also revealed a gene expression increase in VEGFA treated hASCs, most notably on day 14. We also investigated expression profiles of genes related to angiogenesis. qRT-PCR analysis of *VE-CADHERIN* (CD144), which is an endothelial marker, revealed markedly increased expression in VEGFA treated hASCs, whereas in untreated hASCs *VE-CADHERIN* was not detectable until day 14. Moreover, expression of *PECAM-1* (CD31), an additional endothelial marker, was highest in hASCs treated with 20 ng VEGFA at day 3, 7 and 14. Thus, our results showed an upregulation of osteogenesis and osteogenic genes in VEGFA treated hASCs undergoing osteogenic differentiation *in vitro*. In addition, genes that are specific for angiogenesis were likewise upregulated in VEGFA treated hASCs during osteogenic differentiation. The above results suggested that VEGF-receptors were expressed on hASCs undergoing osteogenic differentiation in the presence of VEGFA. qRT-PCR analysis revealed that *VEGF-R2* was expressed from day 0 to day 7 in all groups at similar levels, however expression of *VEGF-R1* could not be detected at any time point. Moreover, no significant differences in the gene expression level were observed between p0 and p1cells (data not shown).

The finding that genes related to angiogenesis were upregulated in hASCs undergoing osteogenesis was somewhat surprising. Therefore, we investigated the initial amount of endothelial cells in freshly isolated hASCs, which could represent a potential contamination. Flow cytometry analysis was performed for $CD31^+$ and $CD45^+$ to identify contaminating endothelial and hematopoietic cells. Neither anti-$CD31^+$/$CD45^+$ nor isotype control antibody analysis identified cells positive for either marker (**Figure 1D**). We therefore believe that it is unlikely that contaminating hematopoietic or endothelial cells influenced our gene expression data, although we do acknowledge that little expression of *PECAM-1* but not *VE-CADHERIN* was detectable in hASCs at day 0.

Osteogenesis is increased in VEGFA treated hASCs *in vivo*

Upon the observation that VEGFA has the potential to increase osteogenesis and angiogenesis of hASCs *in vitro*, we sought to test these effects *in vivo*. We performed critical sized calvarial defects in parietal bones of nude mice and seeded VEGFA treated and untreated hASCs on coral apatite scaffolds. For medical translational scenarios a brief seeding time span would be favorable. For this reason we changed our previous procedure [5] and shortened the incubation time of hASCs on scaffolds to only 20 min before the scaffolds were implanted. To assess cell-attachment, mice (n=3) from each different treatment group (n=9) were harvested 48 hours after surgery and scaffolds were analyzed. As indicated by Hematoxylin staining, a negligible amount of cells were observed in the serum or VEGFA+ serum group (controls), whereas cells were spread throughout the scaffold in the untreated hASC and VEGFA treated hASC group. (**Figure 2, panel A**). The few cells in the control groups could represent cells migrating from the dura mater or pericranium due to the chemoattractant growth factors present in serum. Moreover, DAPI-staining confirmed the cell attachment of hASCs on scaffolds (**Figure 2, panel B**). Having confirmed that hASCs can efficiently attach to the scaffolds, we evaluated proliferation and osteogenic differentiation of hASCs by performing immunohistochemistry for PCNA and RUNX2 (**Figure 2, panels C and D**). Few PCNA positive cells were observed in the control groups. In contrast, a large number of PCNA positive cells were observed in the hASCs and VEGFA+hASCs group, which displayed similar quantities of positive cells distributed in the seeded scaffolds throughout the defects. (**Figure 2, panel C**). Immunohistochemistry for RUNX2 revealed no staining in the control groups, while cells stained positive for RUNX2 in the untreated and VEGFA treated hASCs group (**Figure 2, panel D**). Likewise, nuclear staining was observed within the scaffolds, previously seeded with hASCs.

In order to investigate, whether local application of VEGFA increases hASC bone formation *in-vivo,* healing was first assed by μCT-analysis (**Figure 3, panel A**). μCT-scan time course analysis revealed only minor healing of empty defects at week 8 post-surgery (9.2%). Treatment of defects loaded with serum or VEGFA + serum (controls) revealed degradation of the scaffolds over the time course. For the serum alone group, the fill was 65.7% at week 1 and decreased to 51.1% up to week 8, while it was 61.1% at week 1 with a decrease to 52.9% for VEGFA + serum. In contrast, scaffolds seeded with hASCs revealed a fill of 79.8% at week 8. Finally, local administration of VEGFA to hASC seeded on scaffolds resulted in significant increases in fill as compared to all groups at all time points (95.4% healing at week 8). Since the radiopacity of coral scaffolds on CT-scans imposes limitations on the assessment of calvarial healing, we sought to evaluate the relative contributions of intact scaffolds and regenerated bone to the regenerative construct. To address this question, we sectioned the entire defects and performed H&E staining (**Figure 3, panel B**). H&E staining revealed patchy bone regeneration in the untreated hASC group. However, the VEGFA treated hASCs group exhibited complete or near complete bone regeneration. In contrast, mainly matrices of loose fibrous tissue were observed in the defect area of the controls groups, while ossification was minimal or missing. In order to detect at histological level bone regeneration in the defects, aniline blue staining was performed on every 6^{th} slide (**Figure 4, panel A**). Histomorphometry revealed a significant increase in new bone formation in the hASCs group, which was significantly outperformed (156.5% increase) by the VEGFA + serum group (**Figure 4, panel B**). This trend was accompanied by a substantial decrease in defect width (**Figure 4, panel C**). Moreover, Pentachrome staining did not reveal cartilage tissue formation in the regenerating defects. This suggested that healing most likely occurred through intramembranous ossification (**Figure 4, panel A**). Finally, TRAP staining in the regenerated bone revealed similar amounts of remodeling in both, the hASCs and VEGFA + hASCs group (**Figure 4, panel A**).

Angiogenesis is markedly increased in defects seeded with VEGFA treated hASCs through cell-autonomous and paracrine effects

The increased bone healing capacity of calvarial defects treated with a combination of VEGFA/hASCs could be attributed to an increase in *RUNX2* expression. However, the considerable difference in bone healing capacity observed between untreated and VEGFA treated hASCs prompted us to investigate additional mechanisms, which could be responsible for the increased healing. VEGFA is a well-known inducer of angiogenesis [14] and our *in vitro* data pointed to an upregulation of angiogenic genes during osteogenic differentiation of VEGFA treated hASCs. Therefore we analyzed whether VEGFA treatment of hASCs affected induction of angiogenesis in our calvarial defect model either by stimulating murine endogenous cells or exogenous transplanted hASCs. In order to detect endothelial cells and therefore vessel formation originating from hASCs, we performed immunohistochemistry using specific antibodies for human-CD31/PECAM-1 [28]. After 7 days, staining for human-PECAM-1 revealed sparse vessel formation in the VEGFA treated hASCs group (**Figure 5, panel A**). In contrast, no human-PECAM-1 could be detected in defects treated with hASCs alone (and all other groups). These results indicated that in this model, VEGFA induced cell-autonomous endothelial cell differentiation of hASCs during calvarial healing.

Many studies suggested that hASCs increase angiogenesis through paracrine mechanisms [29-31]. Hence, we performed immunohistochemistry for mouse-CD31/PECAM-1 (**Figure 5, panel A**). In defects treated with serum alone or a combination of serum plus VEGFA, no formation of any vessels was observed. In contrast to what was observed for the human PECAM-1 immunohistochemistry, mouse vessel formation could be detected in defects treated with hASCs alone. Importantly, vessel formation was markedly increased in defects

treated with VEGFA/hASCs. Quantification of vessel surface (**Figure 5, panel B**) or vessel quantity (**Figure 5, panel C**), revealed a dramatic increase of 400% in vessel formation upon VEGFA treatment of hASCs as compared to hASCs alone. Interestingly, vessel formation did not only occur in the scaffold area, but also in the vicinity of the dura mater and regenerating pericranium. At high magnification, erythrocytes were observed in the lumen of the positively stained vessels, which indicated a connection of these newly formed vessels to the vasculature of the host (**Figure 5, panel A**). In a direct comparison of mouse and human endothelial cell differentiation of hASCs and VEGFA+hASCs treated murine calvarial defects it was evident, that significantly more vessels in the defect were of murine origin (**Figure 5, panels A-C**). The mean of detectable vessels per 5x field was 3.2 for human PECAM and 55.8 for mouse PECAM, indicating 17.4x more vessels elicited by paracrine effects. Thus, the detection of human and mouse vessels in defects seeded with VEGFA treated hASCs indicated that they were capable to differentiate to endothelial cells and elicit paracrine angiogenic effects on the murine endogenous host cells.

Co-localization of CD31^{-}/CD45^{-} mASCs^{GFP+} with endothelial cells

Human and mouse PECAM-1 staining at day 7 post-surgery suggested that VEGFA treated hASCs transplanted in calvarial defects did have cell-autonomous and paracrine effects on angiogenesis. In order to investigate this hypothesis more thoroughly and add evidence that hASCs can autonomously differentiate to endothelial cells, as well as, elicit paracrine functions in angiogenesis, we transplanted VEGFA treated CD31^{-}/CD45^{-} mASCs^{GFP+} into calvarial defects. Importantly, FACS sorting was performed to avoid endothelial or hematopoietic cell contamination of the mASCs^{GFP+} cell population. In order to rule out a potential phenotype switch of endothelial cells in culture, stromal cell fractions were sorted before seeding cells in culture (**Figure 6, panel A**). During the harvesting procedure, the CD31+/CD45+ cell population represented 93.3% of the entire cell population, therefore indicating a major contamination of cells other than mASCs before seeding them in culture **(Figure 6, panel A**). Before implantation, fluorescence of the cells was confirmed by microscopy (**Figure 6B**). Seven days after implantation, we evaluated the distribution of VEGFA treated CD31^{-}/CD45^{-} mASC^{GFP+} cells in calvarial defects (**Figure 6, panel B**). In the defect model, the dura mater was left intact and scaffold seeded with CD31^{-}/CD45^{-} mASCs^{GFP+} were positioned cranial of the dura mater. This dissemination did not change at the time of tissue harvest (**Figure 6, panel B**). GFP-positive cells were detected throughout the defect, however there was a layer of cells in the caudal dura mater, where GFP-positive cells were only rarely detected. The proportion of GFP-positive cells within the defect was 43.1% (±7.2%), which was indicative for a paracrine effect of the transplanted CD31-/CD45- mASCsGFP+ cells, since these cells were transplanted into an acellular environment and may allow recruitment of other cells

In order to investigate, whether ASCs would differentiate to endothelial cells we performed immunofluorescence for PECAM-1 to co-localize this surface marker with GFP positive cells using confocal microscopy. As shown in **Figure 6, panel C**, CD31^{-}/CD45^{-} mASC^{GFP+} cells (green) did co-localize with a round vessel structure as indicated by PECAM-1 staining (red). DAPI (blue) was included in the merge to emphasize cell nuclei. This observation supported the hypothesis that hASCs were able to differentiate to endothelial cells.

It must be pointed out that the majority of vessels did not co-localize with CD31^{-}/CD45^{-} mASC^{GFP+} cells. The ratio of the number of vessels that co-localized with CD31^{-}/CD45^{-} mASC^{GFP+} cells as compared to no co-localization was 1:14. Therefore, we could conclude, that both, cell-autonomous and paracrine effects of CD31^{-}/CD45^{-} mASC^{GFP+} cells play a role in angiogenesis initiated by VEGFA-treated ASCs.

DISCUSSION

In the present study, we investigated the effects of VEGFA on the osteogenic differentiation of hASCs *in vitro* and *in vivo* and explored their cell-autonomous and paracrine role on angiogenesis. We could demonstrate, that VEGFA enhanced the osteogenic potential of hASCs. This was accompanied by an increase in angiogenesis. These data highlight a link between osteogenesis and angiogenesis in bone healing conducted by a single growth factor, locally applied on multipotent stem cells.

Orchestration of bone formation is inevitably linked to a crosstalk between osteoblasts and endothelial cells [32]. An important mediator of angiogenesis is VEGFA [33, 34], which is physiologically released during fracture healing [35]. A recent study, which deciphered part of this crosstalk demonstrated that VEGFA is primarily released by osteoblasts, while its action is conducted through endothelial cells [18]. Endothelial cells themselves might increase osteogenesis, given that human endothelial cells can increase alkaline phosphatase activity and Collagen I synthesis of human bone marrow stromal cells via gap junction communication [36]. Moreover, it has been shown that human endothelial cells stimulate osteoprogenitor cell differentiation [37]. Thus, it is tempting to speculate that treatment of hASCs with VEGFA might enhance this crosstalk and thereby increase bone formation.

In addition to the well-known angiogenic effects of VEGFA, a role in osteogenesis has been established during the last years [15-17]. Osteogenic effects of VEGFA on osteoblasts, such as increased bone nodule formation and alkaline phosphatase activity have been reported *in vitro* [15]. Moreover, VEGFA increased bone healing *in vivo*, whereupon delivery of VEGFA was performed with bioerodible polylactic acid depot scaffolds or gene-activated matrices [15, 16].

In contrast to osteoblasts, which represent a committed cell line, hASCs are defined by their multipotency and therefore provided an interesting cell source to study the potential dual functionality of VEGFA during osteogenesis. Similar to our study conducted with hASCs, high expression of VEGFA induced mineralization in multipotent human bone-marrow derived mesenchymal cells (BM-MSCs), whereas expression of soluble VEGF-receptor 1 reduced it [38]. Moreover, Mayer and colleagues also observed a trend of increased angiogenesis during osteogenesis *in vitro* [38]. Although ASCs can be harvested easier and in greater abundance than BM-MSCs, their osteogenic capacity is often regarded inferior to BM-MSCs [39, 40] and was therefore attempted to optimize it with VEGFA in our study. Indeed, would be of interest to verify if treatment with VEGFA also results in increased osteogenic potential of BM-MSCs Support for the hypothesis that hASCs are able to differentiate to both osteoblasts and endothelial cells was generated in a recent study that evaluated hASCs in a rat non-union femur fracture model [28].

The potential for hASCs in angiogenesis has not been defined in detail yet. hASCs can secrete VEGF [29] and act in a manner similar to pericytes to stabilize vessels [41]. We generated evidence here, that the angiogenic effects seen with VEGFA treated hASCs and $CD31^{-}/CD45^{-}$ mASCs $^{GFP+}$ were both of cell-autonomous and paracrine natures, suggesting that both mechanisms may play a role during angiogenesis elicited by ASCs. Interestingly, there is support for both theories, however more data are pointing towards a paracrine role for ASCs during angiogenesis, which is consistent with the favoring ratio for a paracrine role we observed. The ability of hASCs to differentiate into endothelial cells was generated in a study where $CD34^{+}/CD31^{-}$ hASCs were injected in an ischemic femoral artery model [12]. In this paper, co-localization of HLA and CD146 suggested an incorporation of hASCs into the capillaries. Though CD146 does not mark endothelial cells but other cells within the endothelial lineage such as pericytes. In contrast to this study, following the injection of rat

ASCs into an injured rat artery, ASCs did not differentiate into capillaries but contributed to endothelial repair in a paracrine fashion [30]. Concomitantly, Rehman and colleagues showed that ASC-conditioned medium significantly increased the number of human endothelial cells [29] supporting a paracrine pro-angiogenic effect of hASCs. Given our data, it is possible that this effect is accelerated by delivery of VEGFA. Finally, hASCs were shown to have paracrine effects on revascularization after ischemic heart injury [31]. To our knowledge, there is no study that revealed both, cell-autonomous and paracrine mechanisms in the context of angiogenesis related to ASCs.

A criticism of some studies, looking at cell-autonomous ability of hASCs differentiating to endothelial cells is their lack of purity, since during the harvest procedure, endothelial cells were inevitably plated. Thus, we were surprised, that the amount of $CD31^+/CD45^+$ cells in hASCs was not distinguishable from measurement error at passage one. However, this small amount of cells is consistent with previous results obtained by Rubina and colleagues, who reported 0.09% cells positive for CD31/CD144 in their population [42]. Another potential concern would be that endothelial cells would switch their surface marker profile in culture and could therefore not be detected as $CD31^-/CD45^-$. In order to rule this out, we prospectively sorted $mASC^{GFP+}$ cells immediately after the harvest procedure to avoid endothelial contamination in the cell culture.

An important translational aspect of our work was the conclusion, that a shortened incubation time of only 20 min was sufficient for the cells attachment and survival on the scaffolds and resulted in angiogenesis and osteogenesis *in vivo* as seen with hASCs and $CD31^-/CD45^-$ $mASCs^{GFP+}$. Previous studies, including our own work, allowed cell attachment on scaffold for 24 hours or longer [1, 5, 43-45]. Recently, osteogenic differentiated rabbit ASCs (rASCs) were incubated for 2 hours before implantation on scaffolds [46]. The authors demonstrated a dose-dependent increase of rASCs on bone formation. However, they did not verify the successful cell attachment at an early point of time. A clinical translation would require an efficient and fast procedure, which could ideally be done in one operation. Our data are encouraging to meet this goal, but further research has to be done to optimize conditions for a given scaffold to convey bone formation.

The dual role of VEGFA on multipotent hASCs illustrates a potential advantage for utilization of less differentiated cells in bone healing. As mentioned earlier, angiogenesis and osteogenesis are closely linked. A similar concept that stresses the importance of endothelial cells and osteoblasts has been recently reported [47]. After differentiation of endothelial cells and osteoblasts from rat bone marrow cells, scaffolds were pre-seeded with endothelial cells, which prevented ischemic necrosis and increased the mechanical properties of the bone graft [47].

CONCLUSION

In conclusion, our study demonstrated that locally applied VEGFA induces concurrent angiogenesis and osteogenesis to increase bone healing conducted by hASCs. As such, this factor is an excellent candidate to chaperone bone healing through effects on hASCs, and may pave the way for an efficient implementation of these cells in regenerative medicine.

Acknowledgments

The authors would like to thank Dr. Charles K.F. Chan and Dr. Jens P. Volkmer at Stanford University for thoughtful discussions and providing GFP mice. We also thank Antonia Müller for help with FACS sorting. This work was supported by the Oak Foundation, the Hagey Laboratory for Pediatric Regenerative Medicine and NIH R21DE019274 to M.T.L. and the German Research Foundation (DFG BE 4169-1) to B.B.

References

1. Cui L, Liu B, Liu G, et al. Repair of cranial bone defects with adipose derived stem cells and coral scaffold in a canine model. Biomaterials. 2007; 28:5477–5486. [PubMed: 17888508]
2. Halvorsen YD, Franklin D, Bond AL, et al. Extracellular matrix mineralization and osteoblast gene expression by human adipose tissue-derived stromal cells. Tissue engineering. 2001; 7:729–741. [PubMed: 11749730]
3. Zuk PA, Zhu M, Mizuno H, et al. Multilineage cells from human adipose tissue: implications for cell-based therapies. Tissue engineering. 2001; 7:211–228. [PubMed: 11304456]
4. Hicok KC, Du Laney TV, Zhou YS, et al. Human adipose-derived adult stem cells produce osteoid in vivo. Tissue engineering. 2004; 10:371–380. [PubMed: 15165454]
5. Cowan CM, Shi YY, Aalami OO, et al. Adipose-derived adult stromal cells heal critical-size mouse calvarial defects. Nature biotechnology. 2004; 22:560–567.
6. Dudas JR, Marra KG, Cooper GM, et al. The osteogenic potential of adipose-derived stem cells for the repair of rabbit calvarial defects. Annals of plastic surgery. 2006; 56:543–548. [PubMed: 16641633]
7. Hattori H, Sato M, Masuoka K, et al. Osteogenic potential of human adipose tissue-derived stromal cells as an alternative stem cell source. Cells, tissues, organs. 2004; 178:2–12. [PubMed: 15550755]
8. Quarto N, Wan DC, Longaker MT. Molecular mechanisms of FGF-2 inhibitory activity in the osteogenic context of mouse adipose-derived stem cells (mASCs). Bone. 2008; 42:1040–1052. [PubMed: 18420480]
9. Muschler GF, Nakamoto C, Griffith LG. Engineering principles of clinical cell-based tissue engineering. J Bone Joint Surg Am. 2004; 86-A:1541–1558. [PubMed: 15252108]
10. Santos MI, Reis RL. Vascularization in bone tissue engineering: physiology, current strategies, major hurdles and future challenges. Macromol Biosci. 2010; 10:12–27. [PubMed: 19688722]
11. Planat-Benard V, Silvestre JS, Cousin B, et al. Plasticity of human adipose lineage cells toward endothelial cells: physiological and therapeutic perspectives. Circulation. 2004; 109:656–663. [PubMed: 14734516]
12. Miranville A, Heeschen C, Sengenes C, et al. Improvement of postnatal neovascularization by human adipose tissue-derived stem cells. Circulation. 2004; 110:349–355. [PubMed: 15238461]
13. Scherberich A, Galli R, Jaquiery C, et al. Three-dimensional perfusion culture of human adipose tissue-derived endothelial and osteoblastic progenitors generates osteogenic constructs with intrinsic vascularization capacity. Stem cells (Dayton, Ohio). 2007; 25:1823–1829.
14. Olsson AK, Dimberg A, Kreuger J, et al. VEGF receptor signalling - in control of vascular function. Nat Rev Mol Cell Biol. 2006; 7:359–371. [PubMed: 16633338]
15. Street J, Bao M, deGuzman L, et al. Vascular endothelial growth factor stimulates bone repair by promoting angiogenesis and bone turnover. Proceedings of the National Academy of Sciences of the United States of America. 2002; 99:9656–9661. [PubMed: 12118119]
16. Geiger F, Bertram H, Berger I, et al. Vascular endothelial growth factor gene-activated matrix (VEGF165-GAM) enhances osteogenesis and angiogenesis in large segmental bone defects. J Bone Miner Res. 2005; 20:2028–2035. [PubMed: 16234976]
17. Gerber HP, Vu TH, Ryan AM, et al. VEGF couples hypertrophic cartilage remodeling, ossification and angiogenesis during endochondral bone formation. Nat Med. 1999; 5:623–628. [PubMed: 10371499]
18. Clarkin CE, Emery RJ, Pitsillides AA, et al. Evaluation of VEGF-mediated signaling in primary human cells reveals a paracrine action for VEGF in osteoblast-mediated crosstalk to endothelial cells. Journal of cellular physiology. 2008; 214:537–544. [PubMed: 17685428]
19. Street J, Lenehan B. Vascular endothelial growth factor regulates osteoblast survival - evidence for an autocrine feedback mechanism. J Orthop Surg Res. 2009; 4:19. [PubMed: 19527527]
20. Nourse MB, Halpin DE, Scatena M, et al. VEGF induces differentiation of functional endothelium from human embryonic stem cells: implications for tissue engineering. Arterioscler Thromb Vasc Biol. 2010; 30:80–89. [PubMed: 19875721]

21. Rufaihah AJ, Haider HK, Heng BC, et al. Directing endothelial differentiation of human embryonic stem cells via transduction with an adenoviral vector expressing the VEGF(165) gene. J Gene Med. 2007; 9:452–461. [PubMed: 17421060]
22. Okabe M, Ikawa M, Kominami K, et al. 'Green mice' as a source of ubiquitous green cells. FEBS letters. 1997; 407:313–319. [PubMed: 9175875]
23. Quarto N, Longaker MT. FGF-2 inhibits osteogenesis in mouse adipose tissue-derived stromal cells and sustains their proliferative and osteogenic potential state. Tissue engineering. 2006; 12:1405–1418. [PubMed: 16846339]
24. Quarto N, Longaker MT. Differential expression of specific FGF ligands and receptor isoforms during osteogenic differentiation of mouse Adipose-derived Stem Cells (mASCs) recapitulates the in vivo osteogenic pattern. Gene. 2008; 424:130–140. [PubMed: 18718860]
25. Mygind T, Stiehler M, Baatrup A, et al. Mesenchymal stem cell ingrowth and differentiation on coralline hydroxyapatite scaffolds. Biomaterials. 2007; 28:1036–1047. [PubMed: 17081601]
26. Behr B, Panetta NJ, Longaker MT, et al. Different endogenous threshold levels of Fibroblast Growth Factor ligands determine the healing potential of frontal and parietal bones. Bone. 2010
27. Behr B, Leucht P, Longaker MT, et al. Fgf-9 is required for angiogenesis and osteogenesis in long bone repair. Proceedings of the National Academy of Sciences of the United States of America. 2010; 107:11853–11858. [PubMed: 20547837]
28. Shoji T, Ii M, Mifune Y, et al. Local transplantation of human multipotent adipose-derived stem cells accelerates fracture healing via enhanced osteogenesis and angiogenesis. Lab Invest. 2010
29. Rehman J, Traktuev D, Li J, et al. Secretion of angiogenic and antiapoptotic factors by human adipose stromal cells. Circulation. 2004; 109:1292–1298.
30. Takahashi M, Suzuki E, Oba S, et al. Adipose tissue-derived stem cells inhibit neointimal formation in a paracrine fashion in rat femoral artery. Am J Physiol Heart Circ Physiol. 2010; 298:H415–423. [PubMed: 19940081]
31. Cai L, Johnstone BH, Cook TG, et al. IFATS collection: Human adipose tissue-derived stem cells induce angiogenesis and nerve sprouting following myocardial infarction, in conjunction with potent preservation of cardiac function. Stem cells (Dayton, Ohio). 2009; 27:230–237.
32. Brandi ML, Collin-Osdoby P. Vascular biology and the skeleton. J Bone Miner Res. 2006; 21:183–192. [PubMed: 16418774]
33. Keramaris NC, Calori GM, Nikolaou VS, et al. Fracture vascularity and bone healing: a systematic review of the role of VEGF. Injury. 2008; 39(Suppl 2):S45–57. [PubMed: 18804573]
34. Gerstenfeld LC, Cullinane DM, Barnes GL, et al. Fracture healing as a post-natal developmental process: Molecular, spatial, and temporal aspects of its regulation. Journal of cellular biochemistry. 2003; 88:873–884. [PubMed: 12616527]
35. Street J, Winter D, Wang JH, et al. Is human fracture hematoma inherently angiogenic? Clin Orthop. 2000:224–237. [PubMed: 10986998]
36. Villars F, Guillotin B, Amedee T, et al. Effect of HUVEC on human osteoprogenitor cell differentiation needs heterotypic gap junction communication. American journal of physiology. 2002; 282:C775–785. [PubMed: 11880266]
37. Guillotin B, Bourget C, Remy-Zolgadri M, et al. Human primary endothelial cells stimulate human osteoprogenitor cell differentiation. Cell Physiol Biochem. 2004; 14:325–332. [PubMed: 15319536]
38. Mayer H, Bertram H, Lindenmaier W, et al. Vascular endothelial growth factor (VEGF-A) expression in human mesenchymal stem cells: autocrine and paracrine role on osteoblastic and endothelial differentiation. Journal of cellular biochemistry. 2005; 95:827–839. [PubMed: 15838884]
39. Im GI, Shin YW, Lee KB. Do adipose tissue-derived mesenchymal stem cells have the same osteogenic and chondrogenic potential as bone marrow-derived cells? Osteoarthritis and cartilage / OARS. Osteoarthritis Research Society. 2005; 13:845–853.
40. Zaminy A, Ragerdi Kashani I, Barbarestani M, et al. Osteogenic differentiation of rat mesenchymal stem cells from adipose tissue in comparison with bone marrow mesenchymal stem cells: melatonin as a differentiation factor. Iran Biomed J. 2008; 12:133–141. [PubMed: 18762816]

41. Traktuev DO, Merfeld-Clauss S, Li J, et al. A population of multipotent CD34-positive adipose stromal cells share pericyte and mesenchymal surface markers, reside in a periendothelial location, and stabilize endothelial networks. Circulation research. 2008; 102:77–85. [PubMed: 17967785]

42. Rubina K, Kalinina N, Efimenko A, et al. Adipose stromal cells stimulate angiogenesis via promoting progenitor cell differentiation, secretion of angiogenic factors, and enhancing vessel maturation. Tissue engineering. 2009; 15:2039–2050. [PubMed: 19368510]

43. Schliephake H, Zghoul N, Jager V, et al. Effect of seeding technique and scaffold material on bone formation in tissue-engineered constructs. Journal of biomedical materials research. 2009; 90:429–437. [PubMed: 18523951]

44. Wan DC, Siedhoff MT, Kwan MD, et al. Refining retinoic acid stimulation for osteogenic differentiation of murine adipose-derived adult stromal cells. Tissue engineering. 2007; 13:1623–1631. [PubMed: 17518707]

45. Kakudo N, Shimotsuma A, Miyake S, et al. Bone tissue engineering using human adipose-derived stem cells and honeycomb collagen scaffold. Journal of biomedical materials research. 2008; 84:191–197. [PubMed: 17607760]

46. Pieri F, Lucarelli E, Corinaldesi G, et al. Dose-dependent effect of adipose-derived adult stem cells on vertical bone regeneration in rabbit calvarium. Biomaterials. 2010; 31:3527–3535. [PubMed: 20170950]

47. Yu H, VandeVord PJ, Mao L, et al. Improved tissue-engineered bone regeneration by endothelial cell mediated vascularization. Biomaterials. 2009; 30:508–517. [PubMed: 18973938]

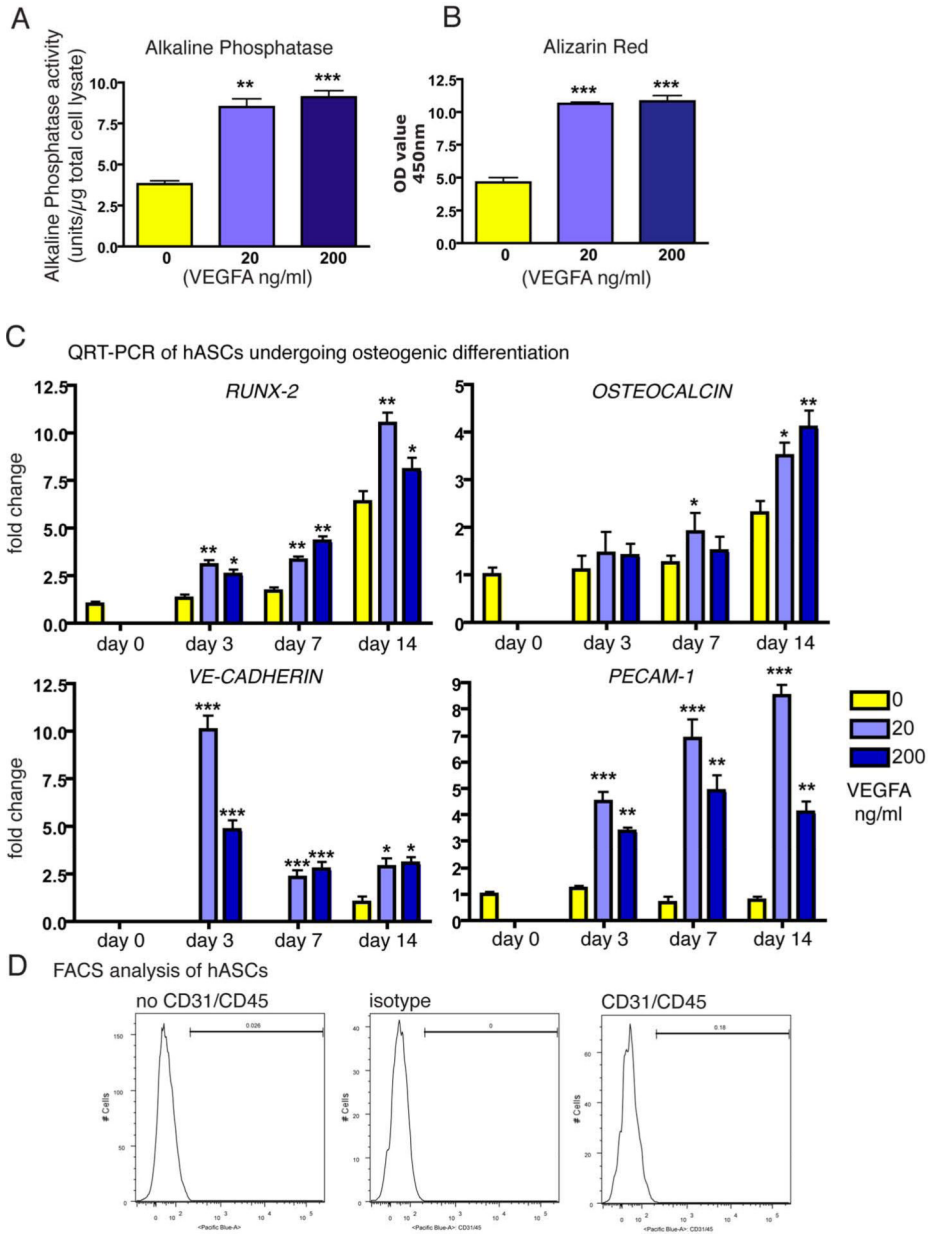

Figure 1.

Effects of VEGFA on hASCs i*n vitro*. **A**, Assay for alkaline phosphatase enzymatic activity and **B**, Alizarin Red staining revealed significant increases upon treating hASCs with 20 or 200 ng/ml VEGFA. **C**, qRT-PCR time course analysis for *RUNX2, OSTEOCALCIN, VE-CADHERIN* and *PECAM-1*. Statistical analysis was conducted using the Student's t-test. P-values: *<0.05, **<0.005 and ***<0.0005 **D**, FACS analysis did not reveal a subpopulation of CD31 or CD45 expressing cells in hASCs. Histogram profiles were comparable among CD31/CD45 incubated versus no antibodies and isotype controls.

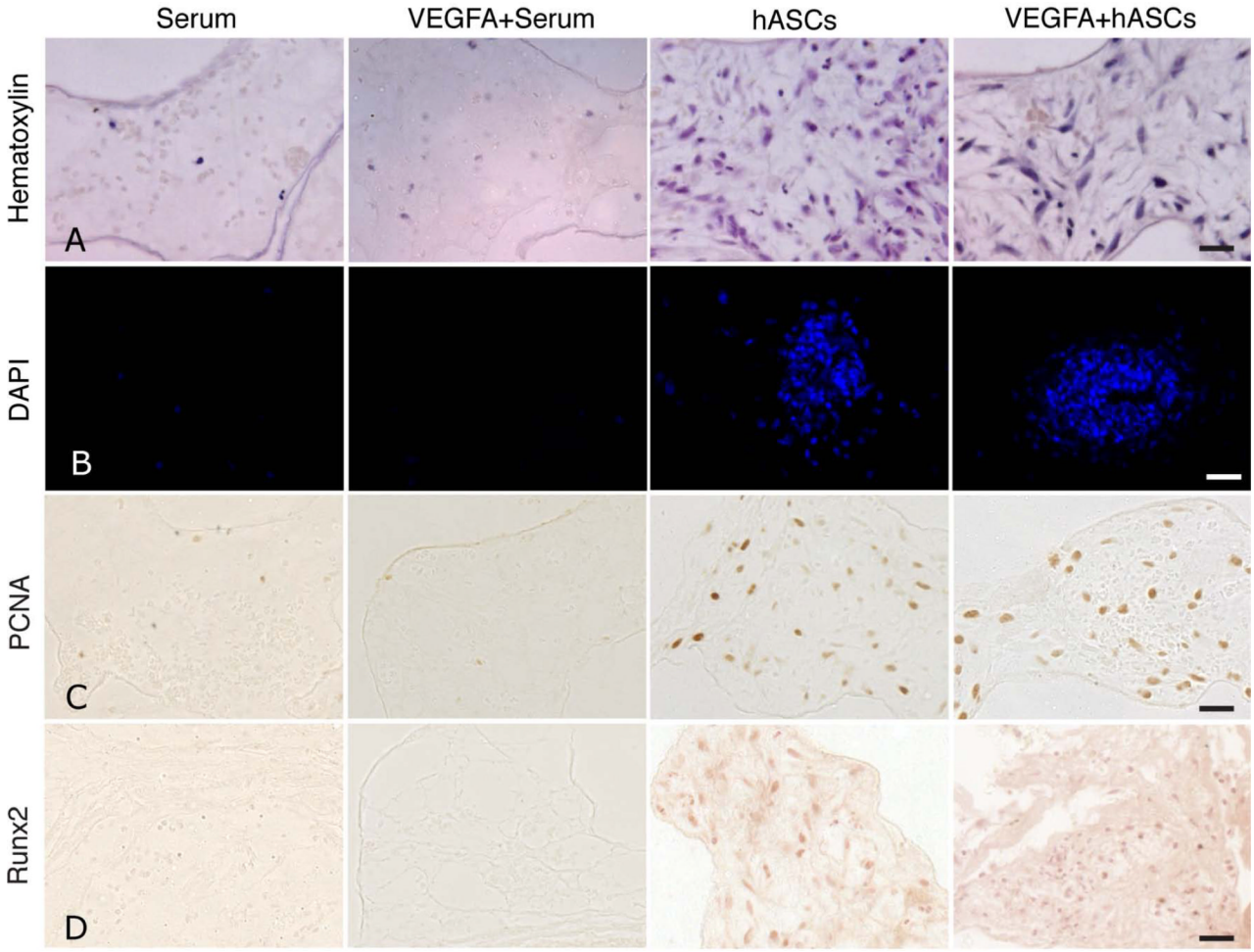

Figure 2.

hASCs attachment to scaffolds and initiation of osteogenic differentiation at 48 hours post defects implantation. **A**, staining for Hematoxylin and **B**, DAPI revealed hASC attachment *in vivo* after 48 hours. **C**, immunohistochemistry for PCNA (**Panel C)**, did not reveal major differences in proliferation between untreated and VEGFA treated hASCs. **D**, immunohistochemistry for RUNX2 revealed similar staining in VEGFA treated hASCs as compared to untreated hASCs, while no staining was observed in the control groups. Scale bars: **A, C, D** 50 μm, **B**, 100 μm.

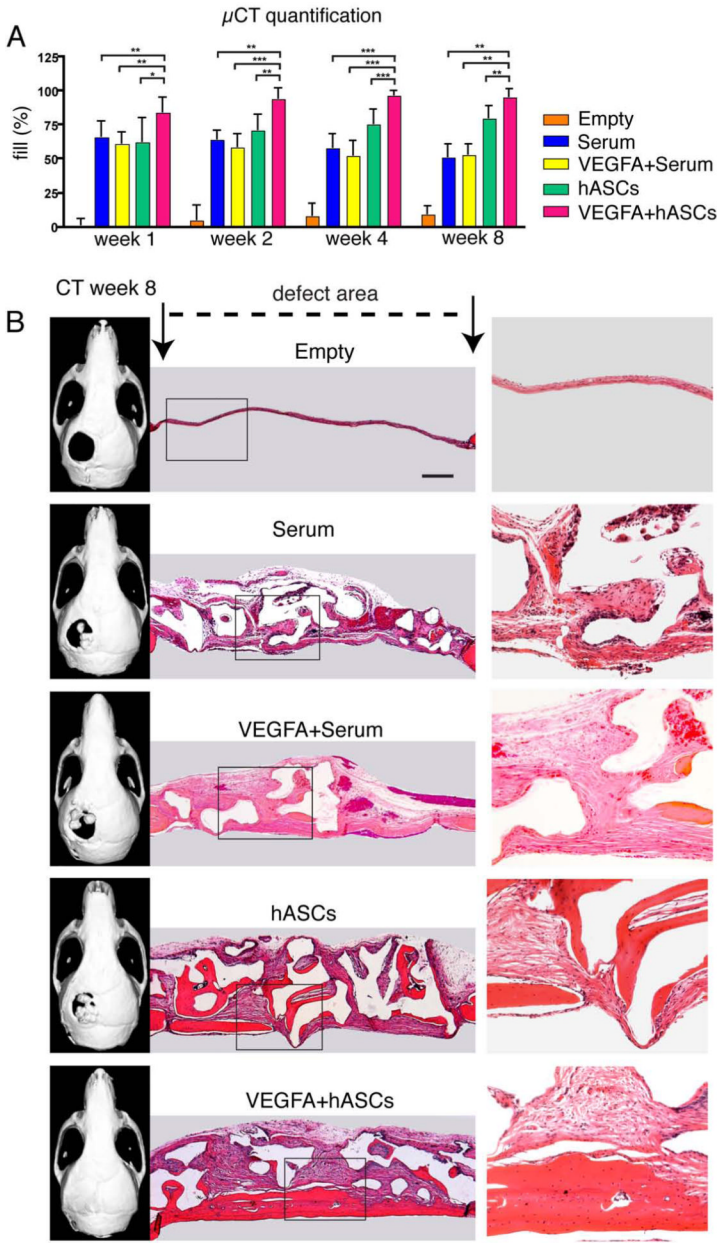

Figure 3.

VEGFA treated hASCs in critical sized calvarial defects. **A**, Quantification of defect fill according to CT results. Statistical analysis was conducted utilizing the Mann-Whitney Test. P-values: *<0.05, **<0.005 and ***<0.0005. **B**, representative CT-scans and corresponding H&E staining at postoperative week 8. Boxed areas are enlarged in the right column. Scale bar: 400 μm

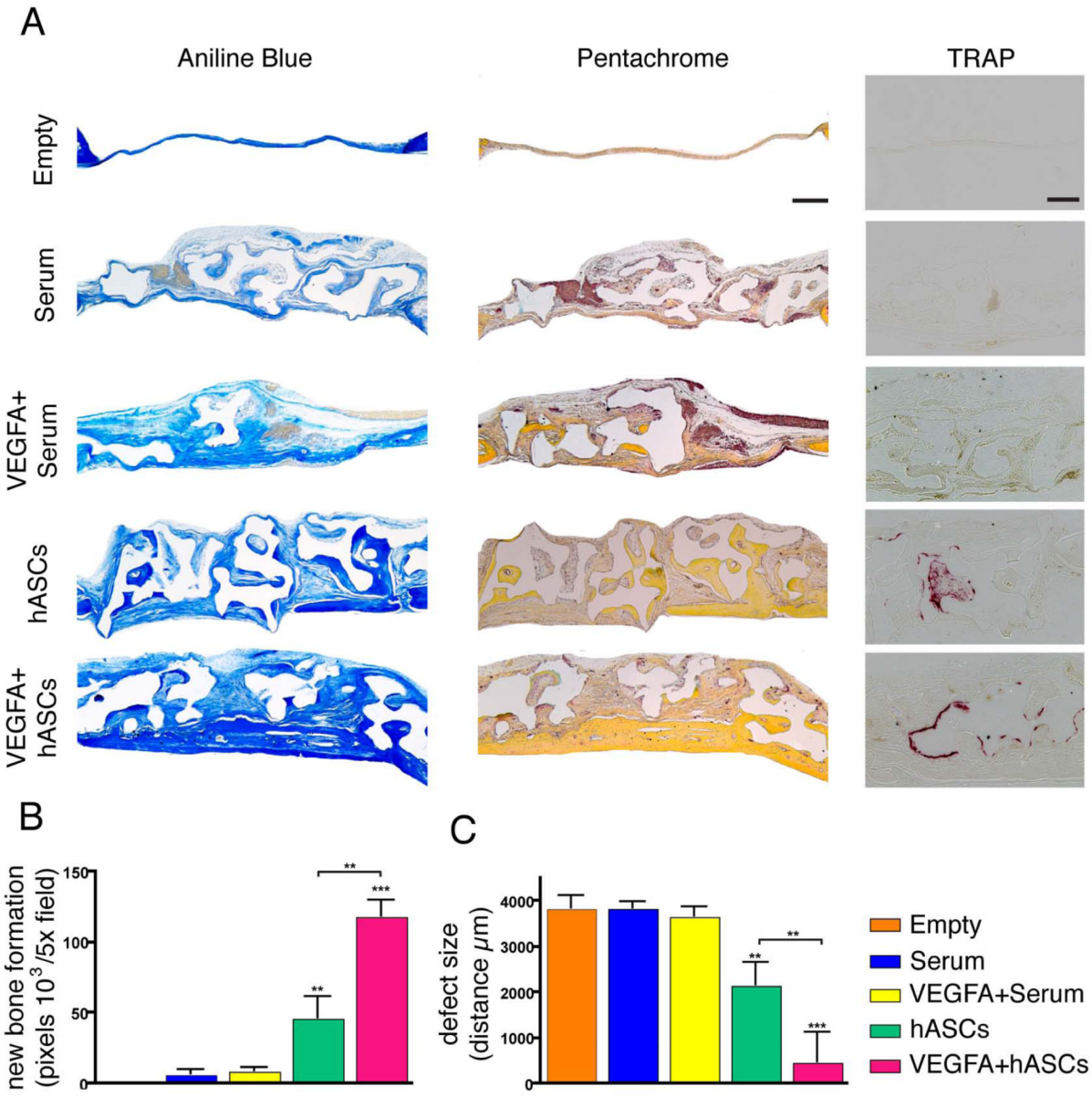

Figure 4.

Bone regeneration and remodeling of calvarial defects. **A**, Aniline Blue, Pentachrome and TRAP staining among the different treatment groups. **B**, Histomorphometry revealed significant increased bone formation in the VEGFA-treated hASCs group. **C**, Conversely, the defect size was significantly decreased in the VEGFA-treated hASCs group. Scale bars: 400μm; TRAP staining 100μm. Statistical analysis was conducted utilizing the Mann-Whitney Test. P-values: **<0.005 and ***<0.0005.

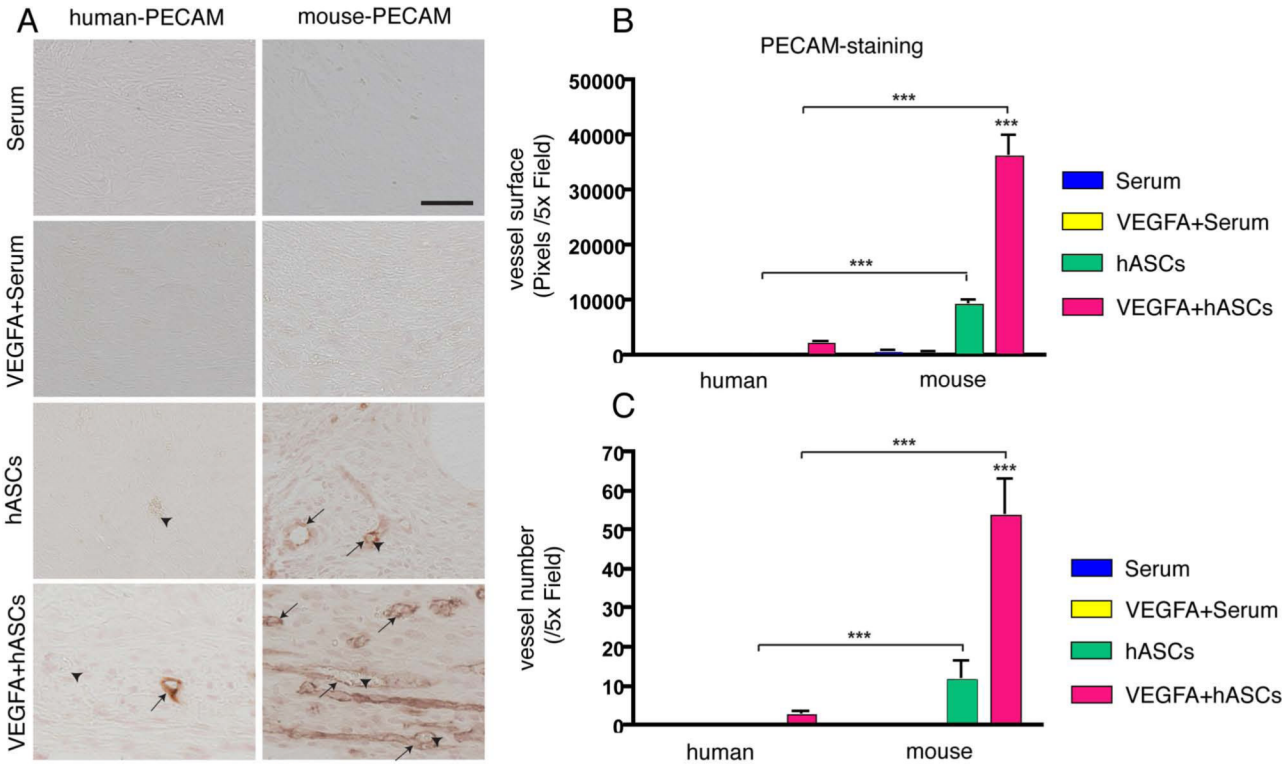

Figure 5.

Angiogenic effects of VEGFA treated and untreated hASC seeded scaffolds via cell autonomous and paracrine effects 7 days after surgery. **A**, Few hASC derived vessels were detected by immunohistochemistry for human-PECAM-1 (left column) in VEGFA treated hASCs, while no hASC derived vessels could be detected in all other groups. Immunohistochemistry for mouse-PECAM-1 (right column) revealed vessel formations in calvarial defects seeded with hASCs. Numerous mouse-PECAM-1 positive vessels were observed in calvarial defects seeded with VEGFA treated hASCs. Arrows indicate PECAM-1 positively stained vessels; arrowheads indicate erythrocytes. Scale bar: 50 μm. **B**, Quantification of the average vessel surface and **C**, average vessel count per 5x field. Statistical analysis was conducted utilizing the Mann-Whitney Test. P-values: **<0.005 and ***<0.0005.

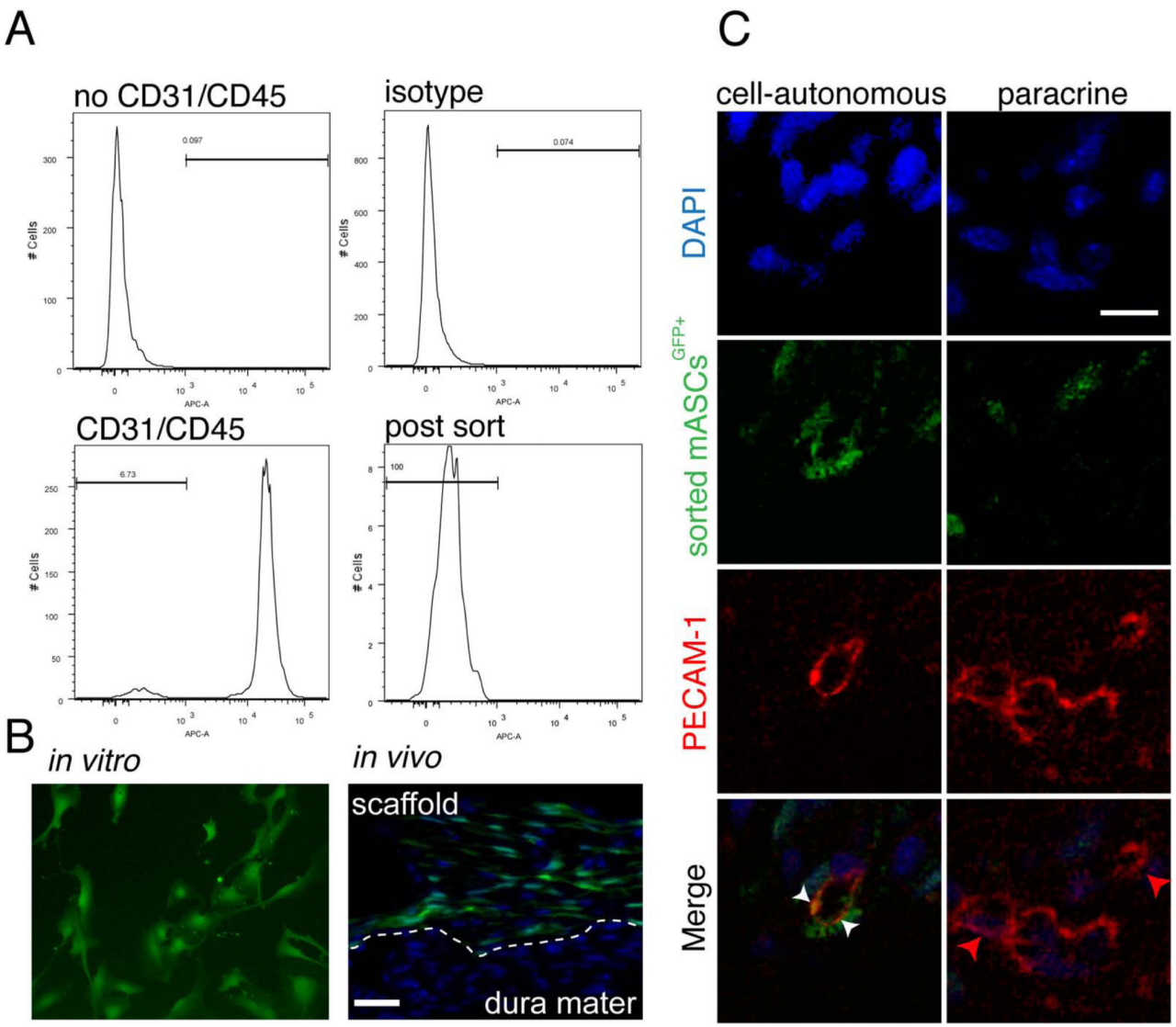

Figure 6.

CD31$^-$/CD45$^-$ mASC^{GFP+} cells contributed to angiogenesis. **A**, FACS sorting of freshly isolated CD31$^-$/CD45$^-$ mASC^{GFP+}. **B**, CD31$^-$/CD45$^-$ mASC^{GFP+} cells were cultured *in vitro*, harvested and seeded on scaffolds. **C**, Co-localization of PECAM-1 and CD31$^-$/CD45$^-$ mASCs^{GFP+} in calvarial defects analyzed by confocal microscopy. Red, green and DAPI merged pictures revealed co-localization of CD31$^-$/CD45$^-$ mASC^{GFP+} and endothelial cells (cell-autonomous; left column). Though vessel formation without contribution of CD31$^-$/CD45$^-$ mASCs^{GFP+} was also observed (paracrine; right column). White arrowheads indicate co-localization, while red arrowheads indicate vessel formation without co-localization. Scale bars: **B:** 50 μm **C:** 10 μm.

TABLE 1

QRT-PCR primer sequences

Gene	Forward primer	Reverse primer
OSTEOCALCIN	GGACTGTGACGAGTTGGCTG	CCGTAGAAGCGCCGATAGG
PECAM-1	AACAGTGTTGACATGAAGAGCC	TGTAAAACAGCACGTCATCCTT
RUNX-2	CCAACCCACGAATGCACTATC	TAGTGAGTGGTGGCGGACATAC
VE-CADHERIN	ATGCACCTGTGTTTGAGAAAAGC	CCTGGATGCGGTATGAGACTT